BIOCHEMISTRY
including biophysical chemistry & molecular biology
Article

Biochemistry **2010,** *49,* 1183–1190 1183
DOI: 10.1021/bi901824a

Spectroscopic Studies of a Sensory Rhodopsin I Homologue from the Archaeon *Haloarcula vallismortis*†

Jin Yagasaki,[‡,§] Daisuke Suzuki,[§] Kunio Ihara,[∥] Keiichi Inoue,[⊥] Takashi Kikukawa,[@] Makoto Sakai,[⊥] Masaaki Fujii,[⊥] Michio Homma,[§] Hideki Kandori,*[,‡] and Yuki Sudo*[,§,#]

[‡]*Department of Frontier Materials, Nagoya Institute of Technology, Showa-ku, Nagoya 466-8555, Japan,* [§]*Division of Biological Science, Graduate School of Science, Nagoya University, Chikusa-ku, Nagoya 464-8602, Japan,* [∥]*Center for Gene Research, Nagoya University, Chikusa-Ku, Nagoya 464-8602, Japan,* [⊥]*Chemical Resources Laboratory, Tokyo Institute of Technology, 4259 Nagatsuta-cho, Midori-ku, Yokohama 226-8503, Japan,* [@]*Division of Biological Sciences, Graduate School of Science, Hokkaido University, Sapporo 060-0810, Japan, and* [#]*PRESTO, Japan Science and Technology Agency* (*JST*)*, 4-1-8 Honcho Kawaguchi, Saitama 332-0012, Japan*

Received October 26, 2009; Revised Manuscript Received January 12, 2010

ABSTRACT: Sensory rhodopsin I (SRI) functions as a dual receptor regulating both negative and positive phototaxis. It transmits light signals through changes in protein−protein interactions with its transducer protein, HtrI. The phototaxis function of *Halobacterium salinarum* SRI (*Hs*SRI) has been well characterized using genetic and molecular techniques, whereas that of *Salinibacter ruber* SRI (*Sr*SRI) has not. *Sr*SRI has the advantage of high protein stability compared with *Hs*SRI and, therefore, provided new information about structural changes and Cl^- binding of SRI. However, nothing is known about the functional role of *Sr*SRI in phototaxis behavior. In this study, we expressed a SRI homologue from the archaeon *Haloarcula vallismortis* (*Hv*SRI) as a recombinant protein which uses all-*trans*-retinal as a chromophore. Functionally important residues of *Hs*SRI are completely conserved in *Hv*SRI (unlike in *Sr*SRI), and *Hv*SRI is extremely stable in buffers without Cl^-. Taking advantage of the high stability, we characterized the photochemical properties of *Hv*SRI under acidic and basic conditions and observed the effects of Cl^- on the protein under both conditions. Fourier transform infrared results revealed that the structural changes in *Hv*SRI were quite similar to those in *Hs*SRI and *Sr*SRI. Thus, *Hv*SRI can become a useful protein model for improving our understanding of the molecular mechanism of the dual photosensing by SRI.

Numerous microorganisms have rhodopsins in their cell membranes, serving as photoreceptors. Bacteriorhodopsin (BR)[1] is one of the most famous membrane proteins and functions as a light-driven proton pump (*1*). The high expression level of BR and the formation of the stable membrane patches helped in the determination of its atomic structure (*1*), which has been used as a guide to analyze the properties and mechanisms of other BR-like proteins and other types of rhodopsins as well. Sensory rhodopsin I (SRI) and sensory rhodopsin II (SRII) form 2:2 complexes with their cognate transducer proteins, halobacterial transducer for SRI (HtrI) and halobacterial transducer for SRII (HtrII), respectively (*2*, *3*), and their complexes work as sensors to transfer signals to the cytoplasm. SRII is specialized as a negative phototaxis receptor (*4*−*6*), while SRI functions as a receptor regulating both negative and positive phototaxis in *Halobacterium salinarum* (*7*−*9*). Because of its high expression level in *Escherichia coli* and stability (*10*−*12*), crystallization of *Natronomonas pharaonis* SRII (*Np*SRII, also called *p*pR) and its cocrystallization with the truncated HtrII were achieved (*2*, *13*, *14*). Also, a number of experiments using electrophysiology (*15*) and EPR (*16*) have been performed on *Np*SRII, which would not have been possible using the homologous protein from *H. salinarum*.

The dark state of *Hs*SRI and its long-lived M-intermediate are responsible for positive and negative phototaxis, respectively, and have absorption maxima at 587 and 373 nm, respectively (*7*). *Hs*SRI is unstable in dilute salt solutions (*17*); therefore, little is known about the molecular mechanisms of interactions between SRI and HtrI, about structural changes, or about the signal relay mechanism. Recently, we characterized a new SRI protein from the eubacterium *Salinibacter ruber* (*Sr*SRI) (*17*). *Sr*SRI is much more stable under various conditions, and therefore, it provided new information about protein structural changes (*18*) and Cl^- binding (*19*). However, no information is available about the functional role of *Sr*SRI in phototaxis, although *S. ruber* cells show negative and positive phototaxis.

In this study, we cloned a gene encoding SRI-like protein from *Haloarcula vallismortis* (*Hv*SRI), which has been discovered as csR3 and sequenced by Kitajima et al. in 1996 (*20*), expressed it in *E. coli*, and succeeded in purifying the highly stable protein. The sequence of *Hv*SRI contains all amino acid residues (N165, H166, D201, and R215) identified as necessary for proper

†This work was supported in part by Grants-in-Aid for Scientific Research (KAKENHI) on Priority Area (Area 477) from the Ministry of Education, Culture, Sports, Science and Technology (MEXT) of Japan. This work was also supported by grants from the Japanese Ministry of Education, Culture, Sports, Science, and Technology to H.K. (19370067 and 20050015) and to Y.S. (20050012).

*To whom correspondence should be addressed. H.K.: telephone and fax, 81 52 735 5207; e-mail, kandori@nitech.ac.jp. Y.S.: telephone, 81 52 789 2993; fax, 81 52 789 3001; e-mail, z47867a@nucc.nagoya-u.ac.jp.

[1]Abbreviations: BR, bacteriorhodopsin; DDM, *n*-dodecyl-β-D-maltoside; HPLC, high-performance liquid chromatography; *Hv*SRI, SRI-like protein from *Haloarcula vallismortis*; $HvSRI_K$, K-intermediate of *Hv*SRI; $HvSRI_M$, M-intermediate of *Hv*SRI; $HvSRI_P$, P-intermediate of *Hv*SRI; PG, L-α-phosphatidylglycerol; SRI, sensory rhodopsin I.

Published on Web 01/12/2010

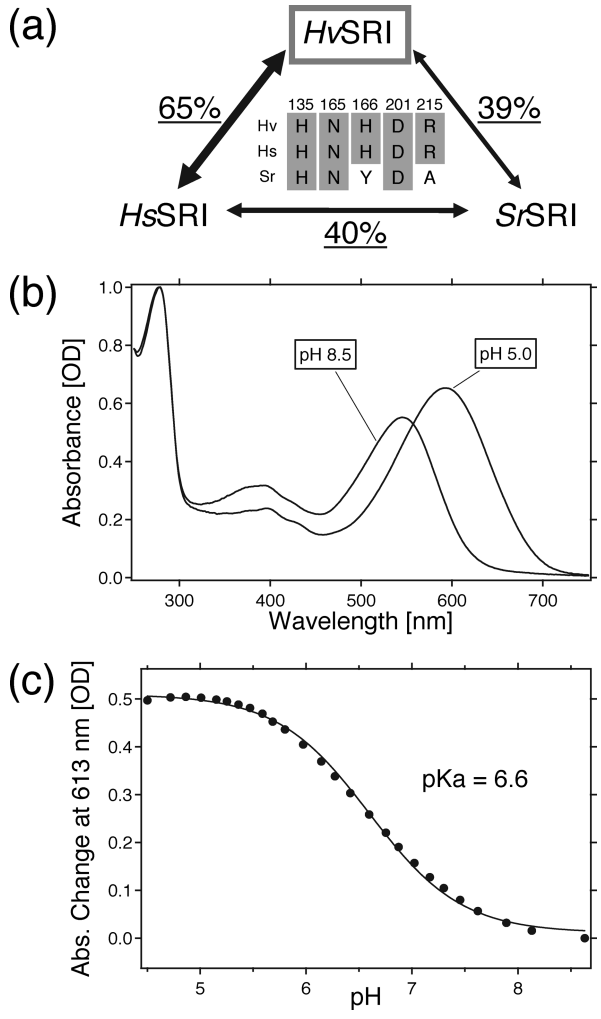

FIGURE 1: (a) Sequence similarities among the three SRI species. Percentages represent the levels of identity between SRI sequences estimated with ClustalW. Five residues important for the phototaxis function are shown in the middle. Residue numbers shown are for *Hv*SRI (GenBank entry D83748). Other accession numbers: *Hs*SRI, *H. salinarum* (L05603); *Sr*SRI, *S. ruber* (3852586). (b) Absorption spectra of *Hv*SRI. The PG-reconstituted sample was resuspended in citric acid buffer (pH 5.0) with 1 M NaCl or in borate buffer (pH 8.5) with 1 M NaCl. The temperature was kept at 25 °C. (c) pH titration curve of the counterion, Asp76, in *Hv*SRI. The titration curve was analyzed using the Henderson−Hasselbalch equation with a single pK_a value.

phototaxis in *Hs*SRI (*9*, *21*−*23*) as well as a histidine residue (H135) important for chloride ion binding (*19*) (Figure 1a). The degree of identity of *Hv*SRI with *Hs*SRI is 65%, which is much higher than that between *Hs*SRI and *Sr*SRI (40%) (*17*). Even with this high degree of homology, the difference in the protein stability with *Hs*SRI is substantial. Utilizing the high stability, we performed the first characterization of *Hv*SRI under acidic and basic conditions.

MATERIALS AND METHODS

Plasmids and Strains. *Ha. vallismortis* was grown aerobically at 37 °C and pH 7.0 in medium with the following composition: 250 g/L NaCl, 20 g/L $MgSO_4 \cdot 7H_2O$, 2 g/L KCl, 0.2 g/L $CaCl_2$, 3.0 g/L Na_3(citrate), and 10 g/L Oxoid pepton (Oxoid Ltd., Hampshire, U.K.). *E. coli* DH5α and BL21(DE3) were used as hosts for DNA manipulation and for protein expression, respectively. The SRI gene was amplified using PCR from the genomic DNA (*24*). Primers were designed by appending an *Nde*I site to the start codon and an *Xho*I site in apposition of the stop codon. The *Nde*I−*Xho*I fragment was digested and ligated to the *Nde*I and *Xho*I sites of the pET21c(+) vector (Novagen, Madison, WI). Consequently, the plasmid encodes six histidines at the C-terminus. This cloning strategy resulted in the following N- and C-terminal peptide sequence: ^{1}MDAV-----TPAD^{236}LEHHHHHH. The constructed plasmid was analyzed using an automated sequencer to confirm the expected nucleotide sequences.

Protein Expression, Purification, and Reconstitution into PG Liposomes. The *Hv*SRI protein sample was prepared as described previously (*17*). Briefly, the protein was expressed in BL21(DE3) cells, solubilized with 1.0% *n*-dodecyl β-D-maltoside (DDM), and then purified using a Ni^{2+}-NTA column (QIAGEN, Valencia, CA) (*25*). The purified samples were then reconstituted into PG liposomes (1:30 *Hv*SRI:PG molar ratio) via removal of the detergent with Bio-Beads (SM2, Bio-Rad, Hercules, CA) (*25*). To monitor the effects of salt on the stability of *Hv*SRI, the PG-reconstituted sample was resuspended in a buffer containing 50 mM Tris-HCl (pH 7.0). Samples were kept at 20 °C, and the absorption spectra were recorded at different time intervals.

pH Titration and High-Performance Liquid Chromatography Analysis. UV−vis spectra were recorded at room temperature using a UV2400PC spectrophotometer with an ISR240A integrating sphere (Shimadzu, Kyoto, Japan). The PG-reconstituted samples were washed and resuspended in a six-component buffer (citric acid, MES, HEPES, MOPS, CHES, and CAPS, whose concentrations were 10 mM each) with 1 M NaCl. The pH of each sample was measured using an F-55 pH-meter with a 9669-C10 glass electrode (HORIBA, Kyoto, Japan). High-performance liquid chromatography (HPLC) analysis was performed as described previously (*19*). The PG-reconstituted sample was analyzed in buffer containing 1 M NaCl and 10 mM citric acid (pH 5.0) or 10 mM borate (pH 8.5). The molar compositions of retinal isomers were calculated from areas of the peaks monitored at 360 nm. The assignment of each peak was performed by comparing it with the HPLC pattern from retinal oximes of authentic all-*trans*- and 13-*cis*-retinals (*26*).

Low-Temperature UV−Vis Spectroscopy. Low-temperature UV−vis spectra were recorded using a V-550DS spectrophotometer (JASCO, Tokyo, Japan) with a cryostat (Optistat DN, Oxford, U.K.) and a temperature controller (ITC502) with liquid nitrogen as the coolant, as described previously (*17*). Each PG-reconstituted sample with 2 mM citric acid (pH 5.0) or 2 mM borate (pH 8.5) was placed on a BaF_2 window and then was dried to a film under pressure reduced with an aspirator. The films were then hydrated with water. To calculate the HvSRI$_M$ minus *Hv*SRI and the HvSRI$_P$ minus HvSRI$_M$ difference spectra, measurements were performed at 200−260 K as follows. The *Hv*SRI film was illuminated with >500 nm light (Y-52) for 2 min, which converts *Hv*SRI to HvSRI$_M$, and then was illuminated through a UV filter (~400 nm light, UG-5, Melles Griot) for 1 min to convert HvSRI$_M$ to HvSRI$_P$. The difference spectra were calculated from the spectra before and after each illumination.

Time-Resolved Flash Spectroscopy. For the flash photolysis experiment on the microsecond time scale (decay of the K-intermediate), the apparatus and the procedure were essentially as described previously (*19*). The purified sample was resuspended in a buffer containing 10 mM citric acid (pH 5.0) or 10 mM borate (pH 8.5) with 1 M NaCl and 0.1% DDM and

was placed in a quartz cell, and then the absorbance was adjusted to ~0.5 OD unit (optical pass length of 2 mm) at the excitation wavelength. The temperature was kept at 25 °C during the measurement. For measurements of the M-intermediate, the conventional flash photolysis apparatus and procedure were essentially as described previously (*27*). The purified sample was resuspended in a buffer containing 10 mM citric acid (pH 5.0) or 10 mM borate (pH 8.5) with 1 M NaCl and 0.1% DDM. Although a phototransient signal could be acquired from a single flash, several kinetic traces were averaged to improve the signal-to-noise (S/N) ratio.

Low-Temperature Fourier Transform Infrared (FTIR) Spectroscopy. Low-temperature FTIR spectroscopy was performed as described previously (*18*). After hydration with H_2O or D_2O, the sample film was placed in a cell mounted in an Oxford Optistat-DN cryostat placed in an FTS-40 spectrometer (Bio-Rad) for *Hv*SRI$_K$ or an FTS-7000 spectrometer (DIGILAB) for *Hv*SRI$_M$. Spectra were constructed from 128 interferograms with a spectral resolution of 2 cm^{-1}. Difference spectra were calculated from spectra before and after illumination. Illumination with 500 nm light at 77 K for 2 min converted *Hv*SRI to *Hv*SRI$_K$, and a subsequent illumination with > 610 nm light (R63) reverted the *Hv*SRI$_K$ back to *Hv*SRI. Thirty-two difference spectra obtained in this way were averaged for each *Hv*SRI$_K$ minus *Hv*SRI spectrum. Illumination with > 500 nm light (Y52) at 260 K for 2 min converted *Hv*SRI to *Hv*SRI$_M$. Six difference spectra obtained in this way were averaged for each *Hv*SRI$_M$ minus *Hv*SRI spectrum.

RESULTS

Protein Expression, Purification, and UV−Vis Spectroscopy. To determine whether the *Hv*SRI gene encodes a functional protein, we cloned and expressed *Hv*SRI in *E. coli* BL21-(DE3) cells. Induction with 0.5 mM isopropyl 1-thio-β-D-galactopyranoside and the addition of retinal (5 μM) changed the color of the transformed cells. Purified *Hv*SRI was reconstituted into PG liposomes, and absorption spectra at pH 5.0 and 8.5 were recorded, as shown in Figure 1b. The absorption maximum of *Hv*SRI is located at 593 nm at pH 5.0 and at 545 nm at pH 8.5. The spectral shift must be due to the protonation of Asp76 of *Hv*SRI, because in all retinal proteins, except for halorhodopsin (HR), the protonated Schiff base is stabilized by an aspartic acid as a counterion (*1*, *28*−*30*). These maximum wavelengths are similar to those of *Hs*SRI (587 and 552 nm, respectively) (*31*) and *Sr*SRI (620 and 558 nm, respectively) (*17*) (Table 1). Alignment of the amino acid sequences with ClustalW reveals that *Hv*SRI is 65 and 39% identical to *Hs*SRI and *Sr*SRI, respectively (Figure 1a). Thus, we were able to express *Hv*SRI as a photoactive membrane-embedded protein.

Retinal Configuration and pK_a of the Counterion. To investigate the properties of *Hv*SRI, HPLC and pH titration experiments were performed. While light-driven ion pumps (e.g., BR and HR) possess both all-*trans*-retinal and 13-*cis*-retinal in the dark (*32*, *33*), the photosensors *Hs*SRI, *Hs*SRII, and *Np*SRII have only all-*trans*-retinal (*26*, *34*). The isomeric state of retinal in *Hv*SRI was predominantly all-*trans* under both acidic and basic conditions (~95.9%), and the retinal configuration was not altered by illumination (480 nm light for 1 min with a Xe lamp), indicating the absence of light or dark adaptation. Thus, the retinal composition of *Hv*SRI is markedly sensory rhodopsin-like (Table 1).

Table 1: Comparison of Characteristics of SRIs

	λ_{max} (acid/base) (nm)	retinal composition	pK_a	stability	Cl^- effects
*Hv*SRI	593/545	all-*trans*	6.6	high	yes
*Hs*SRI	587/552	all-*trans*	7.2	low	not determined
*Sr*SRI	~620/558	all-*trans*	4.3	high	yes

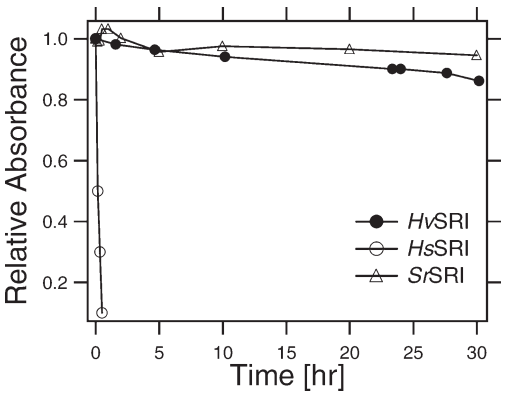

FIGURE 2: Time-dependent absorbance changes of SRI proteins in the absence of NaCl. The samples were reconstituted into PG liposomes and were suspended in a buffer containing 50 mM Tris-HCl (pH 7.0), and the temperature was maintained at 20 °C. The plots for *Hs*SRI and *Sr*SRI were reproduced from previous studies (*17*).

To determine the pK_a value of the counterion Asp76 of *Hv*SRI, we performed pH titration experiments. The titration curve was analyzed using the Henderson−Hasselbalch equation with a single pK_a value, and the value in the unphotolyzed state was estimated to be 6.6 (Figure 1c). This is much closer to that of *Hs*SRI (~7.2) (*35*) than to that of *Sr*SRI (4.3) (*17*) (Table 1), suggesting a structural similarity around the chromophore between *Hv*SRI and *Hs*SRI, but not *Sr*SRI. Because the counterion pK_a values of *Hv*SRI and *Hs*SRI are at neutral pH where these bacteria live, both acidic and basic forms may be considered important for the phototaxis function. Therefore, we characterized *Hv*SRI under both acidic and basic conditions.

Protein Stability. Because of the instability of *Hs*SRI in dilute salt solutions (*17*), little is known about the molecular mechanism for positive phototaxis. The *Sr*SRI protein we characterized previously is highly stable under various conditions compared with *Hs*SRI (*17*). Therefore, *Sr*SRI is useful for characterization of the structural changes of the protein (*18*) and Cl^- binding (*19*). On the other hand, it has several differences from *Hs*SRI, i.e., lack of some functionally important residues (Figure 1a), a lower absorption maximum, a faster overall cycle, and a lower pK_a value of the Schiff base counterion (Table 1). Nevertheless, no structure of any SRI has been determined. Figure 2 shows the stability of *Hv*SRI compared with *Hs*SRI and *Sr*SRI under salt-free conditions, as judged by the light absorbance of the proteins. Fast degradation of *Hs*SRI is obvious, whereas surprisingly, *Hv*SRI exhibited almost the same stability as *Sr*SRI. In addition, PG-reconstituted *Hv*SRI is stable over a wide pH (pH 4−9.5) and temperature (~60 °C) range even in the absence of NaCl and is also expressed in *E. coli* at higher levels (~8 mg/L of culture) than *Sr*SRI (~5 mg/L of culture).

Photocycle Kinetics. Utilizing the high stability and the high expression level, we characterized the photocycle of *Hv*SRI by using low-temperature UV−vis spectroscopy (Figure 3) and flash

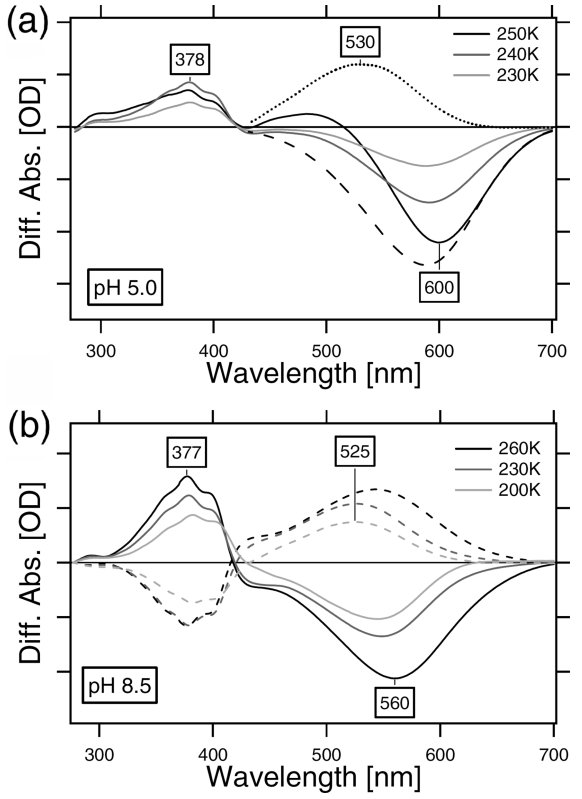

FIGURE 3: Low-temperature UV−vis difference absorption spectra of light-activated *Hv*SRI. The PG-reconstituted sample was suspended in citric acid (pH 5.0) or in borate (pH 8.5) without NaCl. (a) The difference absorption spectra of the pH 5.0 sample at three different temperatures were calculated from the spectra before and after irradiation with > 500 nm light. The dashed line is the simulated absorbance spectrum of the initial state of *Hv*SRI fitted on the slope of the high-wavelength side of the light minus dark difference spectrum at 250 K. The dotted line is the light minus dark difference spectrum minus the simulated initial spectrum, whose peak appears at 530 nm. (b) The difference absorption spectra of the pH 8.5 sample at three different temperatures were calculated from the spectra before and after irradiation with > 500 nm light (—) and from the spectra after the > 500 nm irradiation and after the subsequent UV illumination (---). Each division of the *y*-axis of panels a and b corresponds to 0.05 and 0.1 absorbance unit, respectively.

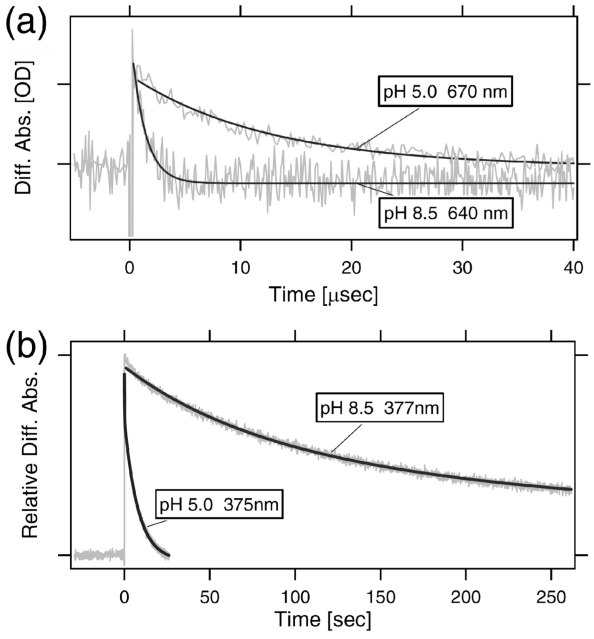

FIGURE 4: Flash-induced kinetic data of *Hv*SRI dissolved in citric acid or in borate containing 1 M NaCl and 0.1% DDM at pH 5.0 or 8.5. (a) Absorbance changes at 670 or 640 nm represent the K-intermediate decay in the acidic or basic form of *Hv*SRI, respectively. The monitoring wavelengths were chosen from the flash-induced difference absorption spectra of *Hv*SRI at each pH over a spectral range from 480 to 725 nm on the nanosecond to microsecond time scale (data not shown). Both sets of data fit well to a single-exponential decay equation, and the half-times were estimated to be 12.7 μs for pH 5.0 and 1.1 μs for pH 8.5. The division of the *y*-axis corresponds to 0.01 absorbance unit. (b) Monitoring the absorbance changes at 375 nm and pH 5.0 or 377 nm and pH 8.5 gave the rates of decay of the M-intermediate. Since the maximal amplitude of the M-intermediate of the acidic form was smaller by a third compared to that of the basic form, the data for the acidic form were renormalized for visual comparison of the decay rates. For all the measurements, the temperature was maintained at 25 °C.

Table 2: Half-Lifetime Values for the K- and M-Intermediates

intermediate	pH	half-lifetime value		
K	5.0	12.7 μs		
	8.5	1.1 μs		
M	5.0	6.2 s (65%)	1.2 s (10%)	54.7 ms (25%)
	8.5	90.5 s (88%)	6.5 s (12%)	

photolysis (Figure 4) experiments. The estimated kinetic parameters are listed in Table 2. For the flash photolysis experiments, a DDM-solubilized sample was used to increase the S/N ratio without inactivation. Low-temperature UV−vis difference spectroscopy reveals that the acidic form of *Hv*SRI has a positive peak at ~500 nm upon illumination at 250 K, which seems to equilibrate with the M-intermediate absorbing at 375 nm (Figure 3a). The light minus dark difference spectrum minus the simulated spectrum of the initial dark state shows the peak at 530 nm; therefore, we denote this intermediate as $HvSRI_{530}$. As the temperature decreases from 250 to 240 K, the $HvSRI_M$ spectral amplitude increases while that of $HvSRI_{530}$ decreases, which suggests that, although $HvSRI_M$ and $HvSRI_{530}$ are in equilibrium, the transition from $HvSRI_M$ to $HvSRI_{530}$ seems to be thermally more favorable. Therefore, $HvSRI_{530}$ is tentatively assigned as the N-intermediate of *Hv*SRI. The basic form of *Hv*SRI has an M-intermediate absorbing at 377 nm as shown in Figure 3b. Since the M-intermediate of basic *Hv*SRI is very stable, we tested whether $HvSRI_M$ forms a P510-like intermediate of *Hs*SRI which is important for negative phototaxis (*7*). UV illumination of the trapped M-intermediate converted it to a red-shifted product with a difference absorbance maximum at 525 nm (Figure 3b). A similar experiment was conducted with the acidic form of *Hv*SRI, and the blue shift was observed as well, although the data were obtained with a low S/N ratio (data not shown).

Using laser flash photolysis, we measured the transient absorption spectra at various time points after excitation on the microsecond time scale, and the wavelengths of maximum absorbance of the K-intermediates were found to be 670 nm at pH 5.0 and 640 nm at pH 8.5 (data not shown). Figure 4a shows the time traces of the absorption changes at 670 nm and pH 5.0 and at 640 nm and pH 8.5. Both curves fit well to a single-exponential decay equation, and the half-times were estimated to be 12.7 μs at pH 5.0 and 1.1 μs at pH 8.5, indicating that the decay rate of the K-intermediate of acidic *Hv*SRI is almost the same as that of *Hs*SRI at pH 6.0 (*36*) and that of basic *Hv*SRI is 21.8-fold faster than that of *Sr*SRI (*19*). The decay curve of the acidic form of $HvSRI_M$ at 375 nm fits well to a triple-exponential decay equation with half-time values of 6.2 s (65%), 1.2 s (10%), and

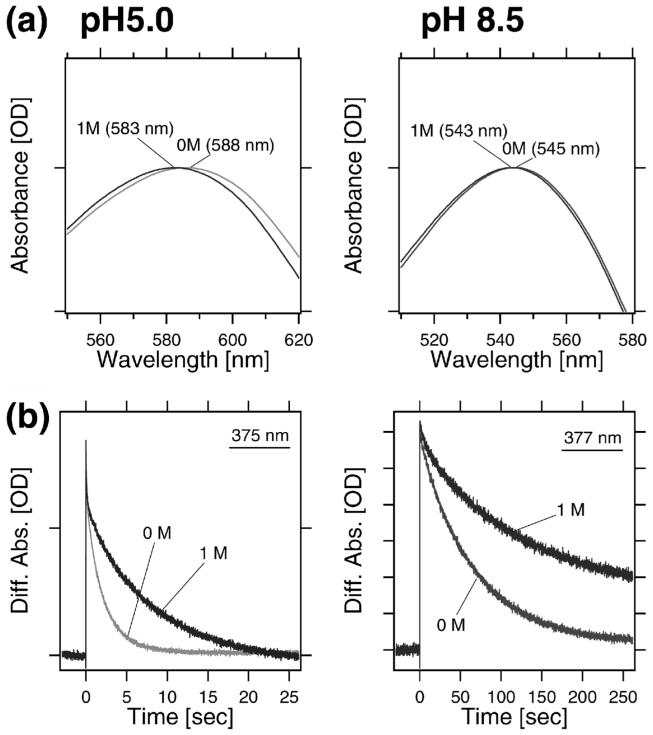

FIGURE 5: (a) Absorption spectra of *Hv*SRI at pH 5.0 (left) or 8.5 (right). The samples was suspended in 0.1% DDM buffer with 1 M NaCl or 0 M NaCl (333 mM Na_2SO_4). The data are shown over a spectral range from 550 to 620 nm for pH 5.0 (from 510 to 580 nm for pH 8.5). (b) Strobe flash-induced kinetic data of *Hv*SRI for pH 5.0 (left) or 8.5 (right) on the second time scale. The samples were suspended in 0.1% DDM buffer with 1 M NaCl or 0 M NaCl (333 mM Na_2SO_4). The curves were fitted by a double-exponential decay equation. The temperature was kept at 25 °C. Each division of the *y*-axis of panels a and b corresponds to 0.2 and 0.01 absorbance unit, respectively.

54.7 ms (25%) (Figure 4b and Table 2), while the decay curve of the basic form of $HvSRI_M$ fits well to a double-exponential decay equation (Figure 4b). The estimated half-time values were 90.5 s (88%) and 6.5 s (12%) (Table 2). $SrSRI_M$ has a 115.5 ms decay half-time under similar conditions, as in the basic form, which means that the M-intermediate decay of *Hv*SRI in the basic form is approximately 800 times slower than that of *Sr*SRI. According to Losi et al (*36*), DDM-dissolved *Hs*SRI at pH 6.0, where its counterion is deprotonated, had lifetime value of 12 s for M-intermediate decay and the undeprotonatable mutant (D76N) had a value of 28 s. Comparing these values with the results for *Hv*SRI described above, we could say that photocycle kinetics of *Hv*SRI is fairly close to that of *Hs*SRI rather than *Sr*SRI.

Effects of Chloride on HvSRI. Figure 5 shows effects of Cl^- on the absorption maxima (a) and photocycle kinetics (b) under acidic and basic conditions. The absorption maximum of *Hv*SRI is shifted from 588 to 583 nm at pH 5.0 (−5 nm) and from 545 to 543 nm at pH 8.5 (−2 nm). As shown in Figure 5b, the M-intermediate decay rates increased by 3.4-fold at pH 5.0 and 1.7-fold at pH 8.5 in the absence of Cl^- compared to those in a 1 M NaCl solution. In the case of *Sr*SRI having a deprotonated counterion (the alkaline form), the λ_{max} is shifted from 542 to 556 nm (+14 nm) in a Cl^--dependent manner (*19*). The M-intermediate decay rate is also increased 5-fold in the absence of Cl^- compared to that in a 1 M NaCl solution (*19*). It should be noted that it is hard to observe the effects of Cl^- on the photochemical properties of *Sr*SRI under the acidic condition (pH < 4.3) because of its instability.

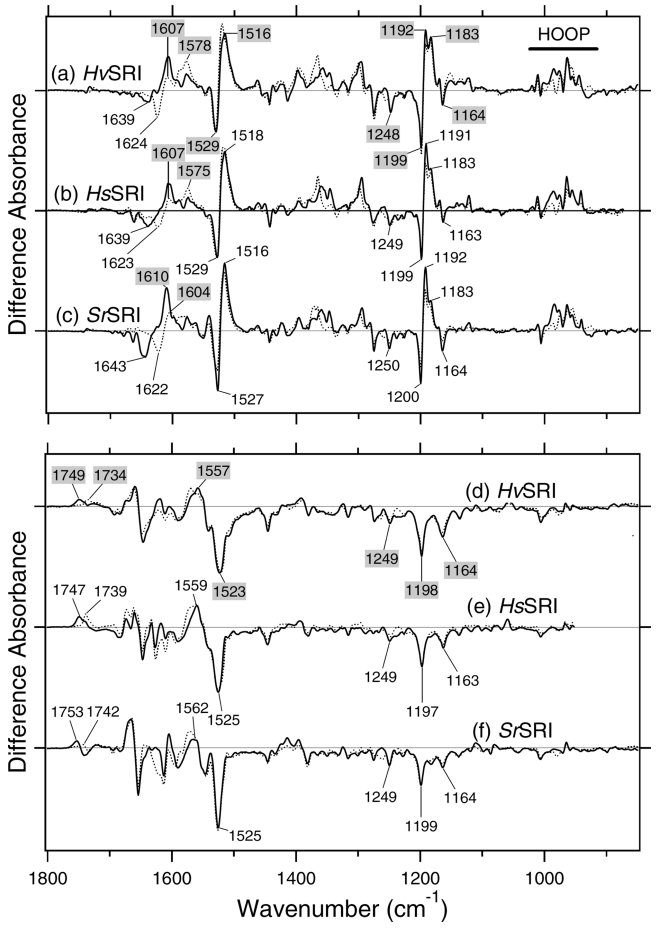

FIGURE 6: (a) Difference infrared spectra ($HvSRI_K$ minus *Hv*SRI) measured at 77 K and pH 8.5 in the 1800−850 cm^{-1} region. Each sample was hydrated with H_2O (—) or D_2O (---). The spectra in panels a and b were multiplied by 4.2 for the sake of comparison. The spectra of *Hs*SRI (b) were deleted at < 872 cm^{-1}. The spectra in panels b and c were reproduced from ref *18* for the sake of comparison. Each division of the *y*-axis corresponds to 0.015 absorbance unit. (d) Difference infrared spectra ($HvSRI_M$ minus *Hv*SRI) measured at 260 K and pH 8.5 in the 1800−850 cm^{-1} region. Each sample was hydrated with H_2O (—) or D_2O (---). The spectra in panel d were multiplied by 0.8 for the sake of comparison. The spectra of *Hs*SRI (e) were deleted at < 951 cm^{-1}. The spectra in panels e and f were reproduced from ref *18* for the sake of comparison. Each division of the *y*-axis corresponds to 0.012 absorbance unit.

FTIR Spectroscopy. To analyze the structural changes of *Hv*SRI during the photocycle, FTIR spectroscopy was performed. The top panel in Figure 6 shows K minus initial state difference FTIR spectra of *Hv*SRI in the 1800−850 cm^{-1} region. The $HsSRI_K$ minus *Hs*SRI and $SrSRI_K$ minus *Sr*SRI spectra are reproduced from ref *18* for the sake of comparison. The bands at 1529(−)/1516(+) cm^{-1} for *Hv*SRI correspond to the ethylenic C=C stretching vibrations of the retinal chromophore. The lower-frequency shift corresponds to the spectral red shift upon formation of the K-intermediate. The bands at 1248(−), 1199(−)/1192(+), and 1183(+)/1164(−) cm^{-1} for *Hv*SRI correspond to the C−C stretching vibrations of the retinal chromophore. The 1639 and 1624 cm^{-1} bands for *Hv*SRI correspond to the C=N stretching vibrations in H_2O and D_2O, respectively. The difference in frequencies between H_2O and D_2O has been regarded as a marker of the strength of hydrogen bonding between the Schiff base and the counterion (*37*−*39*). Frequency differences are 15 cm^{-1} in *Hv*SRI, 16 cm^{-1} in *Hs*SRI (*40*), and 21 cm^{-1} in *Sr*SRI (*18*), all of which are close to the value for

*Np*SRII, 17 cm^{-1} (*25*). In the K-intermediate, this C=N stretching vibration frequency shifts to 1607 cm^{-1} for *Hv*SRI_K, to 1607 cm^{-1} for *Hs*SRI_K, and to 1610 cm^{-1} for *Sr*SRI_K in H_2O. The downshift by D_2O was observed only with *Sr*SRI_K (from 1610 to 1604 cm^{-1}). However, only *Hv*SRI_K and *Hs*SRI_K in D_2O have positive bands at 1578 and 1575 cm^{-1}, respectively, which could be candidates for the C=N stretch vibrations in D_2O.

The bottom panel of Figure 6 shows the M-intermediate minus initial state difference FTIR spectra of *Hv*SRI in the 1800−850 cm^{-1} region. The *Hs*SRI_M minus *Hs*SRI and the *Sr*SRI_M minus *Sr*SRI spectra are reproduced from ref *18* for the sake of comparison. The bands at 1557(+)/1523(−) cm^{-1} for *Hv*SRI correspond to the ethylenic C=C stretching vibrations of the retinal chromophore, and the amide II vibrations also possibly appear here. The negative bands at 1249, 1198, and 1164 cm^{-1} for *Hv*SRI are attributed to the C−C stretching vibrations of the retinal chromophore, where the intensities of the corresponding positive peaks seen in the K-intermediate are much reduced due to the loss of charge at the Schiff base upon deprotonation. When the Schiff base counterion is deprotonated, formation of the M-intermediate accompanies the transfer of a proton from the Schiff base to the counterion. In *Hv*SRI, positive bands at 1749 cm^{-1} in H_2O and at 1734 cm^{-1} in D_2O were observed. Therefore, it is reasonable to assign these bands as the C=O stretching vibrations of Asp76. Thus, the overall signatures of the three SRI spectra upon formation of K- and M-intermediates look very similar to each other, indicating a common structure and structural changes among SRIs upon formation of the K- and M-intermediates.

DISCUSSION

High Stability of HvSRI. Since the initial discovery of SRI in 1982 (*41*, *42*), the signal relay mechanism from SRI to its cognate Htr transducer has become a focus of interest, in part because of its importance to the general understanding of communication between integral membrane proteins, about which little is known. Important advances in understanding the molecular mechanism of negative phototaxis regulated by the SRII−HtrII complex have been made in recent years (*2*, *6*, *15*, *16*). In contrast, little is known about the molecular mechanism of positive phototaxis. In fact, high-resolution crystal structures of BR, HR, SRII, and the SRII−HtrII complex were reported from 1997 through 2006 (*2*, *13*, *14*, *43*, *44*), whereas the structure of SRI has not yet been determined. In 2008, we found and characterized a highly stable SRI homologous protein, *Sr*SRI. However, *Sr*SRI differs in several ways from *Hs*SRI; e.g., *Sr*SRI does not have the His residue on the F-helix conserved among the archaeal SRIs (Figure 1a), which may correlate with the absence of the acidic form of *Sr*SRI, while *Hs*SRI exists as the acidic form at neutral pH. Further, the photoreaction kinetics of free *Sr*SRI are pH-independent, while those of the *Sr*SRI−*Sr*HtrI complex are pH-dependent, completely the opposite of *Hs*SRI (*27*). In this study, we introduced a third SRI species, *Hv*SRI, that has been successfully expressed and purified with good yield from *E. coli* cells as a recombinant protein with high stability (Figure 2). What is the difference that determines the stability of *Hv*SRI in the absence of salt? In 1993, Oesterhelt and co-workers reported that truncation of the C-terminal region of *Hs*SRI results in high levels of protein expression (*45*). Although the C-terminal region of *Hv*SRI may be involved in protein stability, the amino acid sequence is quite different from those of *Hs*SRI and *Sr*SRI. *Hv*SRI and *Sr*SRI do not have a common component that is missing in *Hs*SRI; thus, *Hv*SRI must have a unique strategy for maintaining the integrity of its seven α-helices. Since *Hv*SRI and *Hs*SRI are 65% identical, differences in their sequences are limited. Further study will be required to understand the high stability of *Hv*SRI.

Comparison of Photochemical Properties of HvSRI with Those of HsSRI and SrSRI. We demonstrate here that the absorption maximum and pK_a value of the counterion of *Hv*SRI are quite similar to those of *Hs*SRI, but not those of *Sr*SRI (Figure 1 and Table 1). The photocycle kinetics of *Hv*SRI are also more similar to those of *Hs*SRI than of *Sr*SRI. In *Hs*SRI, it was reported that a histidine residue, His166, plays an important role in the pathways of proton transfer both to and from the Schiff base (*22*). The histidine residue is conserved in *Hv*SRI but not in *Sr*SRI (Figure 1a); therefore, this residue is a strong candidate for the determinant of the differences. In fact, the M-intermediate was observed even in the acidic form of *Hv*SRI (Figure 3) where the counterion Asp76 is protonated (Figure 1). It could be explained by the transfer of a proton from the Schiff base of *Hv*SRI_{593} to the His166 homologue upon formation of the M-intermediate, like in *Hs*SRI. In addition, we observed here the effects of Cl^- on the absorption maximum and photocycling rate of *Hv*SRI both under acidic and alkaline conditions (Figure 5). The acceleration of M-intermediate decay and the shift of the absorption maximum without Cl^- are also observed in *Sr*SRI, although *Hv*SRI shows the Cl^--dependent blue shift that is different from that of *Sr*SRI [14 nm red shift (*19*)]. In the case of SRII from *N. pharaonis*, no effect of Cl^- on absorption maximum (*46*) or photocycle kinetics (*47*) was reported previously, although the spectral shift was observed under the acidic conditions (pH < 3) in a chloride-dependent manner (*46*). These data strongly suggest that binding of Cl^- to sensory rhodopsin I is widely conserved among members of the sensory rhodopsin I protein family, unlike in SRII, and assumed to be an important property for the functional differentiation between SRI and SRII. In fact, the putative Cl^- binding site, His135, is also conserved in *Hs*SRI and *Sr*SRI (Figure 1a). The binding seems to be independent of the protonation state of Asp76 (Figure 5).

Structural Changes Revealed by FTIR Spectroscopy. We compared the hydrogen-out-of-plane (HOOP) vibration region (1050−850 cm^{-1}) of *Hv*SRI_K minus the *Hv*SRI difference FTIR spectra with those of *Hs*SRI, *Sr*SRI, *Np*SRII, BR, and the BR-T mutant. We have reported that the triple mutant, BR-T, is able to form a signaling complex with HtrII and can mediate phototaxis responses like SRII (*48*); therefore, BR-T is regarded as an SRII-like protein. Several peaks appear upon formation of the K-intermediate of *Hv*SRI as well as *Hs*SRI, *Sr*SRI (Figure 6a), SRII (*25*), and BR-T (*49*), suggesting that the structural changes in the retinal chromophore seem to be essential for the sensory rhodopsins. Thus, the low-temperature FTIR spectroscopy upon formation of K- and M-intermediates showed that the difference spectra of *Hv*SRI are quite similar to those of *Hs*SRI as well as those of *Sr*SRI (Figure 6), in particular with the structural changes of the retinal chromophre (HOOP, C=C, and C−C vibrations). However, in the region above 1600 cm^{-1}, all three spectra exhibited differences probably due to the large effects of amide bands derived from the different protein moieties among three SRIs, especially in M-intermediates.

In conclusion, we have succeeded in purifying a highly stable SRI-like protein from *Ha. vallismortis*, and it can be expressed well in *E. coli* as a recombinant protein. The functionally important residues of *Hs*SRI are completely conserved in *Hv*SRI

(unlike in *Sr*SRI). Spectroscopic studies revealed that the photochemical properties and structural changes of *Hv*SRI are more similar to those of *Hs*SRI than to those of *Sr*SRI. Utilizing the high stability, the characteristics of *Hv*SRI under the acidic and basic conditions were investigated, and Cl^- effects were observed under both acidic and basic conditions. Thus, *Hv*SRI will become a useful protein for further elucidation of the molecular mechanism of the dual photosensing by SRI. In addition to the cloning and expression of HtrI for *Hv*SRI, further studies are required for investigation of the SRI−HtrI system.

ACKNOWLEDGMENT

We are very grateful to Dr. Tomomi Kitajima-Ihara for technical assistance with the DNA manipulation. We also thank Mr. Junya Yamada for technical assistance with the time-resolved laser spectroscopy.

REFERENCES

1. Lanyi, J. K. (2004) Bacteriorhodopsin. *Annu. Rev. Physiol. 66*, 665–688.
2. Gordeliy, V. I., Labahn, J., Moukhametzianov, R., Efremov, R., Granzin, J., Schlesinger, R., Buldt, G., Savopol, T., Scheidig, A. J., Klare, J. P., and Engelhard, M. (2002) Molecular basis of transmembrane signalling by sensory rhodopsin II-transducer complex. *Nature 419*, 484–487.
3. Chen, X., and Spudich, J. L. (2002) Demonstration of 2:2 stoichiometry in the functional SRI-HtrI signaling complex in *Halobacterium* membranes by gene fusion analysis. *Biochemistry 41*, 3891–3896.
4. Takahashi, T., Tomioka, H., Kamo, N., and Kobatake, Y. (1985) A photosystem other than PS370 also mediates the negative phototaxis of *Halobacterium halobium*. *FEMS Microbiol. Lett. 28*, 4.
5. Zhang, W., Brooun, A., Mueller, M. M., and Alam, M. (1996) The primary structures of the Archaeon *Halobacterium salinarium* blue light receptor sensory rhodopsin II and its transducer, a methyl-accepting protein. *Proc. Natl. Acad. Sci. U.S.A. 93*, 8230–8235.
6. Sasaki, J., and Spudich, J. L. (2008) Signal transfer in haloarchaeal sensory rhodopsin-transducer complexes. *Photochem. Photobiol. 84*, 863–868.
7. Spudich, J. L., and Bogomolni, R. A. (1984) Mechanism of colour discrimination by a bacterial sensory rhodopsin. *Nature 312*, 509–513.
8. Hoff, W. D., Jung, K. H., and Spudich, J. L. (1997) Molecular mechanism of photosignaling by archaeal sensory rhodopsins. *Annu. Rev. Biophys. Biomol. Struct. 26*, 223–258.
9. Sasaki, J., Phillips, B. J., Chen, X., Van Eps, N., Tsai, A. L., Hubbell, W. L., and Spudich, J. L. (2007) Different dark conformations function in color-sensitive photosignaling by the sensory rhodopsin I-HtrI complex. *Biophys. J. 92*, 4045–4053.
10. Shimono, K., Iwamoto, M., Sumi, M., and Kamo, N. (1997) Functional expression of *pharaonis* phoborhodopsin in *Escherichia coli*. *FEBS Lett. 420*, 54–56.
11. Sudo, Y., Iwamoto, M., Shimono, K., and Kamo, N. (2001) *Pharaonis* phoborhodopsin binds to its cognate truncated transducer even in the presence of a detergent with a 1:1 stoichiometry. *Photochem. Photobiol. 74*, 489–494.
12. Sudo, Y., Yamabi, M., Iwamoto, M., Shimono, K., and Kamo, N. (2003) Interaction of *Natronobacterium pharaonis* phoborhodopsin (sensory rhodopsin II) with its cognate transducer probed by increase in the thermal stability. *Photochem. Photobiol. 78*, 511–516.
13. Luecke, H., Schobert, B., Lanyi, J. K., Spudich, E. N., and Spudich, J. L. (2001) Crystal structure of sensory rhodopsin II at 2.4 angstroms: Insights into color tuning and transducer interaction. *Science 293*, 1499–1503.
14. Royant, A., Nollert, P., Edman, K., Neutze, R., Landau, E. M., Pebay-Peyroula, E., and Navarro, J. (2001) X-ray structure of sensory rhodopsin II at 2.1-Å resolution. *Proc. Natl. Acad. Sci. U.S.A. 98*, 10131–10136.
15. Jiang, X., Zaitseva, E., Schmidt, M., Siebert, F., Engelhard, M., Schlesinger, R., Ataka, K., Vogel, R., and Heberle, J. (2008) Resolving voltage-dependent structural changes of a membrane photoreceptor by surface-enhanced IR difference spectroscopy. *Proc. Natl. Acad. Sci. U.S.A. 105*, 12113–12117.
16. Doebber, M., Bordignon, E., Klare, J. P., Holterhues, J., Martell, S., Mennes, N., Li, L., Engelhard, M., and Steinhoff, H. J. (2008) Salt-driven equilibrium between two conformations in the HAMP domain from *Natronomonas pharaonis*: The language of signal transfer? *J. Biol. Chem. 283*, 28691–28701.
17. Kitajima-Ihara, T., Furutani, Y., Suzuki, D., Ihara, K., Kandori, H., Homma, M., and Sudo, Y. (2008) Salinibacter sensory rhodopsin: Sensory rhodopsin I-like protein from a eubacterium. *J. Biol. Chem. 283*, 23533–23541.
18. Suzuki, D., Sudo, Y., Furutani, Y., Takahashi, H., Homma, M., and Kandori, H. (2008) Structural changes of *Salinibacter* sensory rhodopsin I upon formation of the K and M photointermediates. *Biochemistry 47*, 12750–12759.
19. Suzuki, D., Furutani, Y., Inoue, K., Kikukawa, T., Sakai, M., Fujii, M., Kandori, H., Homma, M., and Sudo, Y. (2009) Effects of chloride ion binding on the photochemical properties of *Salinibacter* sensory rhodopsin I. *J. Mol. Biol. 392*, 48–62.
20. Kitajima, T., Hirayama, J., Ihara, K., Sugiyama, Y., Kamo, N., and Mukohata, Y. (1996) Novel bacterial rhodopsins from *Haloarcula vallismortis*. *Biochem. Biophys. Res. Commun. 220*, 341–345.
21. Olson, K. D., Zhang, X. N., and Spudich, J. L. (1995) Residue replacements of buried aspartyl and related residues in sensory rhodopsin I: D201N produces inverted phototaxis signals. *Proc. Natl. Acad. Sci. U.S.A. 92*, 3185–3189.
22. Zhang, X. N., and Spudich, J. L. (1997) His166 is critical for active-site proton transfer and phototaxis signaling by sensory rhodopsin I. *Biophys. J. 73*, 1516–1523.
23. Jung, K. H., and Spudich, J. L. (1998) Suppressor mutation analysis of the sensory rhodopsin I-transducer complex: Insights into the color-sensing mechanism. *J. Bacteriol. 180*, 2033–2042.
24. Marmur, J. (1961) Procedure for isolation of deoxyribonucleic acid from micro-organisms. *J. Mol. Biol. 3*, 11.
25. Kandori, H., Shimono, K., Sudo, Y., Iwamoto, M., Shichida, Y., and Kamo, N. (2001) Structural changes of *pharaonis* phoborhodopsin upon photoisomerization of the retinal chromophore: Infrared spectral comparison with bacteriorhodopsin. *Biochemistry 40*, 9238–9246.
26. Imamoto, Y., Shichida, Y., Hirayama, J., Tomioka, H., Kamo, N., and Yoshizawa, T. (1992) Chromophore configuration of pharaonis phoborhodopsin and its isomerization on photon absorption. *Biochemistry 31*, 2523–2528.
27. Sudo, Y., Okada, A., Suzuki, D., Inoue, K., Irieda, H., Sakai, M., Fujii, M., Furutani, Y., Kandori, H., and Homma, M. (2009) Characterization of a signaling complex composed of sensory rhodopsin I and its cognate transducer protein from the eubacterium *Salinibacter ruber*. *Biochemistry 48*, 10136–10145.
28. Haupts, U., Tittor, J., and Oesterhelt, D. (1999) Closing in on bacteriorhodopsin: Progress in understanding the molecule. *Annu. Rev. Biophys. Biomol. Struct. 28*, 367–399.
29. Kataoka, M., Kamikubo, H., Tokunaga, F., Brown, L. S., Yamazaki, Y., Maeda, A., Sheves, M., Needleman, R., and Lanyi, J. K. (1994) Energy coupling in an ion pump. The reprotonation switch of bacteriorhodopsin. *J. Mol. Biol. 243*, 621–638.
30. Brown, L. S., Dioumaev, A. K., Needleman, R., and Lanyi, J. K. (1998) Connectivity of the retinal Schiff base to Asp85 and Asp96 during the bacteriorhodopsin photocycle: The local-access model. *Biophys. J. 75*, 1455–1465.
31. Olson, K. D., Deval, P., and Spudich, J. L. (1992) Absorption and photochemistry of sensory rhodopsin-I: pH effects. *Photochem. Photobiol. 56*, 1181–1187.
32. Pettei, M. J., Yudd, A. P., Nakanishi, K., Henselman, R., and Stoeckenius, W. (1977) Identification of retinal isomers isolated from bacteriorhodopsin. *Biochemistry 16*, 1955–1959.
33. Kamo, N., Hazemoto, N., Kobatake, Y., and Mukohata, Y. (1985) Light and dark adaptation of halorhodopsin. *Arch. Biochem. Biophys. 238*, 90–96.
34. Scharf, B., Hess, B., and Engelhard, M. (1992) Chromophore of sensory rhodopsin II from *Halobacterium halobium*. *Biochemistry 31*, 12486–12492.
35. Spudich, J. L. (1995) Transducer protein HtrI controls proton movements in sensory rhodopsin I. *Biophys. Chem. 56*, 165–169.
36. Losi, A., Braslavsky, S. E., Gartner, W., and Spudich, J. L. (1999) Time-resolved absorption and photothermal measurements with sensory rhodopsin I from *Halobacterium salinarum*. *Biophys. J. 76*, 2183–2191.
37. Aton, B., Doukas, A. G., Narva, D., Callender, R. H., Dinur, U., and Honig, B. (1980) Resonance Raman studies of the primary photochemical event in visual pigments. *Biophys. J. 29*, 79–94.
38. Baasov, T., Friedman, N., and Sheves, M. (1987) Factors affecting the C=N stretching in protonated retinal Schiff base: A model study for bacteriorhodopsin and visual pigments. *Biochemistry 26*, 3210–3217.
39. Gilson, H. S., Honig, B. H., Croteau, A., Zarrilli, G., and Nakanishi, K. (1988) Analysis of the factors that influence the C=N stretching

frequency of polyene Schiff bases. Implications for bacteriorhodopsin and rhodopsin. *Biophys. J. 53*, 261–269.
40. Furutani, Y., Takahashi, H., Sasaki, J., Sudo, Y., Spudich, J. L., and Kandori, H. (2008) Structural changes of sensory rhodopsin I and its transducer protein are dependent on the protonated state of Asp76. *Biochemistry 47*, 2875–2883.
41. Bogomolni, R. A., and Spudich, J. L. (1982) Identification of a third rhodopsin-like pigment in phototactic *Halobacterium halobium*. *Proc. Natl. Acad. Sci. U.S.A. 79*, 6250–6254.
42. Tsuda, M., Hazemoto, N., Kondo, M., Kamo, N., Kobatake, Y., and Terayama, Y. (1982) Two photocycles in *Halobacterium halobium* that lacks bacteriorhodopsin. *Biochem. Biophys. Res. Commun. 108*, 970–976.
43. Luecke, H., Schobert, B., Richter, H. T., Cartailler, J. P., and Lanyi, J. K. (1999) Structure of bacteriorhodopsin at 1.55 Å resolution. *J. Mol. Biol. 291*, 899–911.
44. Kolbe, M., Besir, H., Essen, L. O., and Oesterhelt, D. (2000) Structure of the light-driven chloride pump halorhodopsin at 1.8 Å resolution. *Science 288*, 1390–1396.
45. Ferrando-May, E., Brustmann, B., and Oesterhelt, D. (1993) A C-terminal truncation results in high-level expression of the functional photoreceptor sensory rhodopsin I in the archaeon *Halobacterium salinarium*. *Mol. Microbiol. 9*, 943–953.
46. Shimono, K., Kitami, M., Iwamoto, M., and Kamo, N. (2000) Involvement of two groups in reversal of the bathochromic shift of *pharaonis* phoborhodopsin by chloride at low pH. *Biophys. Chem. 87*, 225–230.
47. Iwamoto, M., Hasegawa, C., Sudo, Y., Shimono, K., Araiso, T., and Kamo, N. (2004) Proton release and uptake of *pharaonis* phoborhodopsin (sensory rhodopsin II) reconstituted into phospholipids. *Biochemistry 43*, 3195–3203.
48. Sudo, Y., and Spudich, J. L. (2006) Three strategically placed hydrogen-bonding residues convert a proton pump into a sensory receptor. *Proc. Natl. Acad. Sci. U.S.A. 103*, 16129–16134.
49. Sudo, Y., Furutani, Y., Spudich, J. L., and Kandori, H. (2007) Early photocycle structural changes in a bacteriorhodopsin mutant engineered to transmit photosensory signals. *J. Biol. Chem. 282*, 15550–15558.